Absorption Spectra, Photophysical Properties, and Redox Behavior of Ruthenium(II) Polypyridine Complexes Containing Accessory Dipyrromethene−BF_2 Chromophores

Maurilio Galletta,[†] Fausto Puntoriero,[†] Sebastiano Campagna,*[,†] Claudio Chiorboli,[§] Manuel Quesada,[‡] Sebastien Goeb,[‡] and Raymond Ziessel*[,‡]

Dipartimento di Chimica Inorganica, Chimica Analitica e Chimica Fisica, Università di Messina, Via Sperone 31, 98166 Messina, Italy, ISOF-CNR, Sezione di Ferrara, and Dipartimento di Chimica, Università di Ferrara, Via Borsari 46, 44100 Ferrara, Italy, and Laboratoire de Chimie Moléculaire, Ecole de Chimie, Polymères, Matériaux (ECPM), Université Louis Pasteur (ULP), 25 rue Becquerel, 67087 Strasbourg Cedex 02, France

Received: December 6, 2005; In Final Form: January 13, 2006

The six multichromophoric species **1**−**6**, containing the potentially luminescent Ru(II) polypyridine subunits and 4,4-difluoro-4-bora-3a,4a-diaza-s-indacene fluorophores (dipyrromethene−BF_2 dyes, herein after called bodipy), have been prepared and their absorption spectra, luminescence properties (both at room temperature in fluid solution and at 77 K in rigid matrix), and redox properties have been investigated *(for the structural formulas of all the compounds, see Figure 1*). For comparison purposes, also the same properties of the bodipy-based free ligands have been examined. Three of the multichromophoric species (**1**−**3**) are based on the $Ru(bpy)_3$-type metal subunit, whereas **4**−**6** are based on the $Ru(terpy)_2$-type metal subunit. Transient absorption spectroscopy at room temperature of all the compounds has also been performed. The absorption spectra of all the metal complexes show features that can be assigned to the Ru(II) polypyridine subunits and to the bodipy centers. In particular, the lowest energy spin-allowed $\pi-\pi^*$ transition of the bodipy groups dominates the visible region, peaking at about 530 nm. All the new complexes exhibit a rich redox behavior, with reversible processes attributed to specific sites, indicating a small perturbation of each redox center and therefore highlighting the supramolecular nature of the multichromophoric assemblies. Despite the good luminescence properties of the separated components, **1**−**6** do not exhibit any luminescence at room temperature; however, transient absorption spectroscopy evidences that for all of them a long-lived (microsecond time scale) excited state is formed, which is identified as the bodipy-based triplet state. Pump−probe transient absorption spectroscopy suggests that such a triplet state is formed from the promptly prepared bodipy-based $^1\pi-\pi^*$ state in most cases by the intervention of a charge-separated level. At 77 K, all the complexes except complex **1** exhibit the bodipy-based fluorescence, although with a slightly shortened lifetime compared to the corresponding free ligand(s), and **4**−**6** also exhibit a phosphorescence assigned to the bodipy subunits. Phosphorescence of bodipy species had never been reported in the literature to the best of our knowledge: in the present cases we propose that it is an effective decay process thanks to the presence of the ruthenium heavy atom and of the closely lying ^{3}MLCT state of the $Ru(terpy)_2$-type subunits.

Introduction

Multichromophoric species are quite interesting from several viewpoints. For example, they can exhibit photoinduced intercomponent electron and/or energy transfer processes, possibly leading to valuable functions such as charge separation and/or energy migration.[1] The study of such processes and functions has been and continues to be fruitful in terms of both fundamental knowledge (e.g., for experimental verification of electron and energy transfer theories)[2] and applicative reasons (e.g., for the development of synthetic systems for artificial photosynthesis).[3]

A potential way to design molecules suitable for such applications is to connect a donor component, having strong absorbance at the excitation wavelength, to an acceptor that displays good emissive properties. An added requirement is that some type of internal barrier has to be inserted to prevent the donor−acceptor structure acting as a single "large molecule".[4] This barrier can be imposed by twisting the molecular axis such that the donor and acceptor units are no longer coplanar, because this has the effect of preventing the system from forming extended orbitals.[5]

Among the many stable and strongly luminescent dyes available, 4,4-difluoro-4-bora-3a,4a-diaza-s-indacene derivatives (trade name bodipy[6]) appear to be particularly well suited for the design of new dual-dye systems.[7] In particular, the fluorescence properties of bodipy chromophores can be tailored and tuned by a variety of different substitution patterns both on the pseudo-meso position and on the pyrrole ring.[8−10] The availability of sophisticated bodipy-based structures offers the possibility to tackle specific problems linked to (i) sensing of protons[11] or other cations[12−15] by optoelectronic switching, (ii) light-harvesting in porphyrin-based arrays[16] and (iii) Stokes' shift discrimination in energy transfer based on molecular modules.[17] On the other hand ruthenium(II) tris-bipyridine and ruthenium(II) bis-terpyridine complexes exhibit well-established redox and optical properties related to the presence of an electron rich metal center and electron accepting polypyridine ligands.[18,19]

[†] Università di Messina.
[§] Università di Ferrara.
[‡] Université Louis Pasteur.

10.1021/jp057094p CCC: $33.50 © 2006 American Chemical Society
Published on Web 03/09/2006

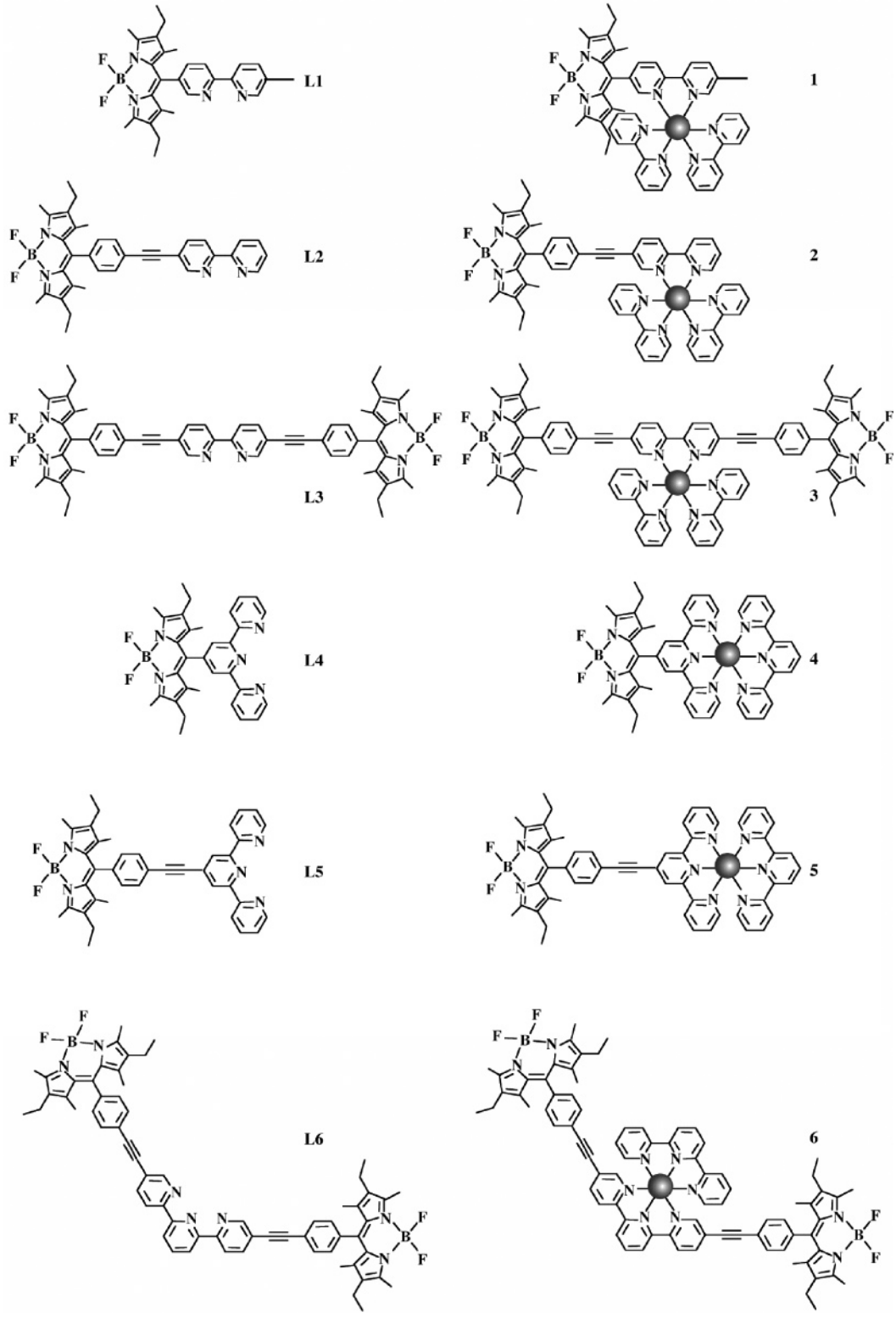

Figure 1. Structural formulas of free ligands and metal complexes. The ruthenium complexes are dications and for each complex two hexafluorophosphate anions are present.

Here we report the synthesis, the absorption spectra, the photophysical properties (both at room temperature in fluid solution and at 77 K in rigid matrix), and the redox behavior of six new ruthenium(II) polypyridine complexes covalently linked to pyrromethene−BF_2 (bodipy) chromophores. In these species, two well-known classes of luminophores, the Ru(II) polypyridine family and the pyrromethene−BF_2 dyes, are therefore linked by a covalent bond so that interesting photoinduced intercomponent processes are expected. The structural formulas of the species studied are shown in Figure 1, together with the abbreviations used. The same properties of the free ligands are also reported, for comparison purposes. The presence of two methyl groups on the bodipy core and in close proximity with the chelating platform induces a twist of the bodipy subunits with respect to the fragments carrying the metal-based chromophores and prevents a complete conjugation between the

TABLE 1: Spectroscopic and Photophysical Data[a]

		luminescence					
		298 K				77 K	
compound	absorption λ_{max}, nm (ϵ, $M^{-1}cm^{-1}$)	λ_{max}, nm	τ, ns	Φ	τ^b	λ_{max}, nm	τ
1	238 (34100); 288 (69400) 453 (13400); 532 (36100)				8 μs		
2	242 (39390); 287 (76750) 396 (12240); 455 (14710) 523 (61340)				10 μs	536	5 ns
3	235 (74300); 286 (81100) 370 (70600); 523 (86700)				9 μs	535	6 ns
4	273 (34800); 307 (43250) 489 (17100); 531 (24900)				10 μs	540 795	6 ns 12 ms
5	276 (52800); 310 (73100) 494 (47700); 523 (66100)				8 μs	536 774	5 ns 50 ms
6	272 (71700); 337 (67200) 372 (58000); 523 (89600)				30 μs	540 774	4 ns 50 ms
L1	292 (13200); 376 (3600) 529 (39800)	544	4	0.69[c]		547	8 ns
L2	241 (22760); 322 (55220) 396 (7970); 527 (87904)	540	4	0.70[c]		536	7 ns
L3	359 (81500); 522 (133400)	536	5	0.87[c]		536	7 ns
L4	280 (24500); 378 (7800) 529 (62700)	546	6	0.48[c]		540	8 ns
L5	278 (199800); 371 (8300) 527 (64700)	540	4	0.70[c]		536	7 ns
L6	284 (37500); 336 (70800) 527 (114700)	542	4	0.89[c]		535	6 ns

[a] For the absorption, the maxima (or shoulders) of the spin-allowed ligand-centered and/or MLCT bands are given. The absorption and the room temperature emission data are in CH_2Cl_2 for **L1**−**L6** and in CH_3CN for **1**−**6**. The 77 K luminescence data are in butyronitrile solution. [b] These data refer to the lifetime of the lowest, nonemissive excited state, measured by transient absorption spectroscopy (see text). [c] Data from ref 21.

various subunits. Preliminary information dealing with some properties of a few compounds reported here has already been communicated.[20]

Results

Synthesis and some properties of the free ligands **L1**−**L6** have been recently described.[21] The already published properties (redox, absorption and room temperature luminescence data) are included here in the various tables (see later) for comparison purposes, as well as the free ligands properties investigated here for the first time, such as the 77 K luminescence properties and the transient absorption data. Ligands built from a bipyridine unit ($\mathbf{L}_1$, $\mathbf{L}_2$ and $\mathbf{L}_3$) were complexed using a classical procedure with stoichiometric amounts of $[Ru(bipy)_2Cl_2]\cdot 2H_2O$[22] as a metal precursor. For the terpyridine based ligands ($\mathbf{L}_4$, $\mathbf{L}_5$ and $\mathbf{L}_6$), a suitable synthetic route uses *cis*-Cl−[Ru(terpy)(DMSO)Cl_2][23] as a metal salt. To ensure a good yield, the metal precursor was previously dehalogenated with $AgBF_4$ (2.2 equiv) and the resulting methanol solution was allowed to react with the free ligand under anhydrous and anaerobic conditions. All complexes were isolated as the hexafluorophosphate salts by column chromatography and recrystallization from adequate solvents. Their molecular structures were unambiguously assigned by NMR, FT-IR, electrospray mass spectroscopy, and elemental analysis.

The new compounds **1**−**6** exhibit a quite intense absorption in the visible, dominated by a sharp band with a maximum between 520 and 535 nm and by a broader band with a lower intensity with a maximum between 450 and 500 nm (ϵ of the band maxima in the range 1×10^4 to 2×10^5 M^{-1} cm^{-1}). Intense absorption bands are also present in the UV region (ϵ in the range 1×10^4 to 1×10^5 M^{-1} cm^{-1}). The relevant absorption data are collected in Table 1. Figures 2−4 show the absorption spectra of compounds **3**, **5**, and **6**, respectively. The redox behavior of **1**−**6** is quite rich: the compounds indeed undergo several oxidation and reduction processes, generally reversible. Table 2 collects the redox data, and Figure 5 shows the cyclic voltammograms of complexes **5** and **6**.

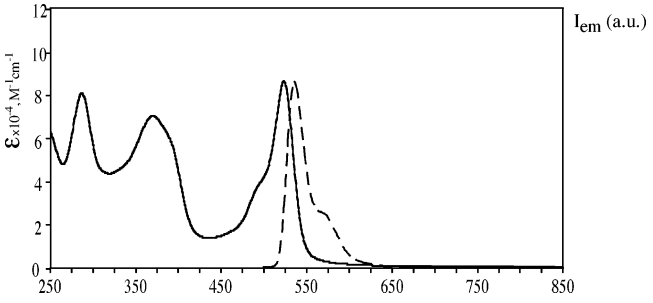

Figure 2. Absorption (in acetonitrile, solid line) and 77 K emission (in butyronitrile, dashed line) spectra of **3**.

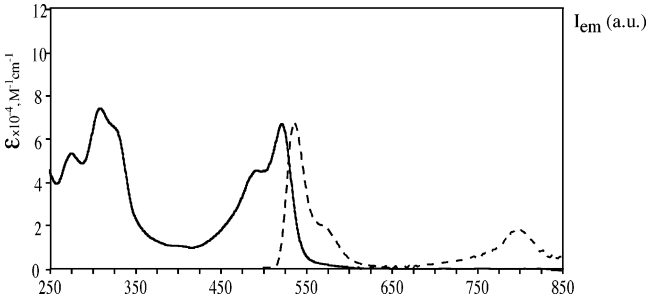

Figure 3. Absorption (in acetonitrile, solid line) and 77 K emission (in butyronitrile, dashed line) spectra of **5**.

Whereas the free ligands **L1**−**L6** exhibit fluorescence both at room temperature in fluid solution and at 77 K in rigid matrix, in all the cases with lifetimes between 1 and 10 ns, not one of the metal complexes is luminescent at room temperature in fluid solution. However, nanosecond transient absorption spectroscopy indicates that an excited state with a relatively long lifetime (in the microsecond time scale in deoxygenated acetonitrile) is

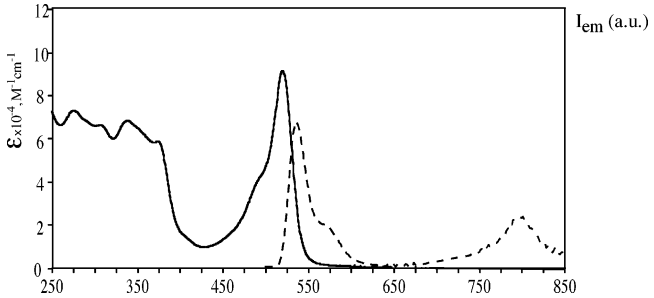

Figure 4. Absorption (in acetonitrile, solid line) and 77 K emission (in butyronitrile, dashed line) spectra of **6**.

TABLE 2: Redox Data[a]

compound	$E_{1/2ox}$,V vs SCE	$E_{1/2red}$, V vs SCE
1	+1.08; +1.40	−1.07; −1.15
		−1.38; −1.63
2	+1.01; +1.38	−1.16; −1.37 [2];
		−1.56
3	+0.99 [2]; +1.43	−1.00; −1.14;
		−1.35 [2]; −1.55
4	+1.07; +1.41	−1.02; −1.30;
		−1.65
5	+0.99; +1.34	−1.14; −1.36; −1.55
6	+0.99 [2]; +1.44;	−1.06; −1.33 [2];
		−1.48; −1.60
$[Ru(bpy)_3]^{2+}$	+1.27	−1.34; −1.54; −1.79
$[Ru(terpy)_2]^{2+}$	+1.30	−1.27; −1.52
L1	+1.08	−1.33
L2	+1.05	−1.34
L3	+1.00 [2]	−1.34 [2]; −1.73
L4	+1.12 (irrev)	−1.27
L5	+1.08 (irrev)	−1.35
L6	+1.00 [2]	−1.37 [2]

[a] Potentials determined by cyclic voltammetry in deoxygenated anhydrous CH_3CN for the metal complexes **1**−**6** and in deoxygenated anhydrous CH_2Cl_2 for the free ligands **L1**−**L6**, containing 0.1 M $TBAPF_6$, at a solute concentration range of 1.5×10^{-3} M, at 20 °C. Potentials were standardized using ferrocene (Fc) as an internal reference and converted to SCE assuming that $E_{1/2}(Fc/Fc^+) = +0.38$ V ($\Delta E_p = 70$ mV) vs SCE. The error in half-wave potentials is ±10 mV. When the redox process is irreversible, the peak potential (E_{ap} or E_{cp}) are quoted. The numbers in parentheses refer to the number of exchanged electrons; when not specified, the process involves one electron. Data for the free ligands are from ref 21.

formed for all the complexes in these conditions. At 77 K in rigid matrix, all the metal complexes except **1** exhibit a short-lived luminescence (nanosecond time scale) quite similar to that exhibited by the corresponding **L1**−**L6** free ligands. Compounds **4**−**6** also exhibit an additional long-lived, red-shifted luminescence (ms time scale) in these conditions. All the luminescence data are gathered in Table 1, which also shows the lifetime of the lowest, nonemissive long-lived excited state measured by transient absorption spectroscopy; Figures 2−4 show the luminescence spectra of compounds **3**, **5**, and **6**, respectively.

Time-resolved pump−probe transient absorption spectroscopy, performed at room temperature on the metal complexes, evidenced for **2**−**6** two successive fast decay processes leading to a long-lived excited-state whose spectroscopic signature is equivalent to that found by nanosecond flash photolysis (see above). For **1**, only a single fast decay is evidenced by pump−probe spectroscopy.

Discussion

Molecular Characterization. The fingerprint of the proton NMR spectra of the complexes is the well-defined pattern corresponding to each fragment present in the molecule;

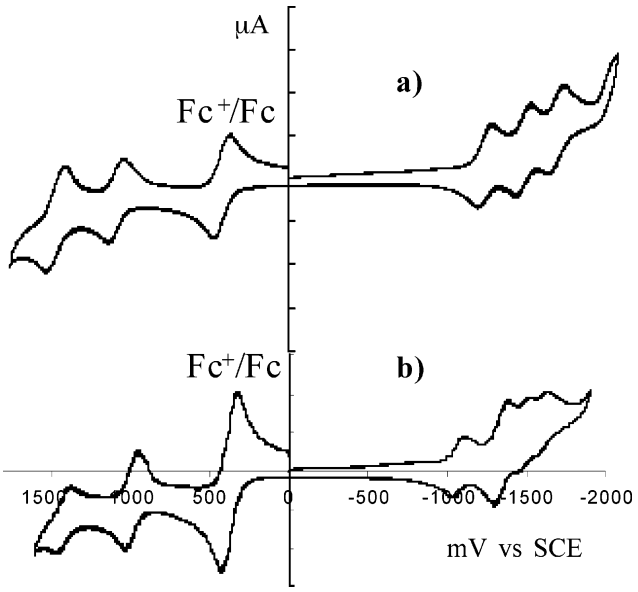

Figure 5. Cyclic voltamogramm measured in anhydrous acetonitrile using tetrabutylammonium hexafluorophosphate as supporting electrolyte: (a) complex **5**; (b) complex **6**. Fc accounts for ferrocene and a scanning rate of 200 mV/s was used.

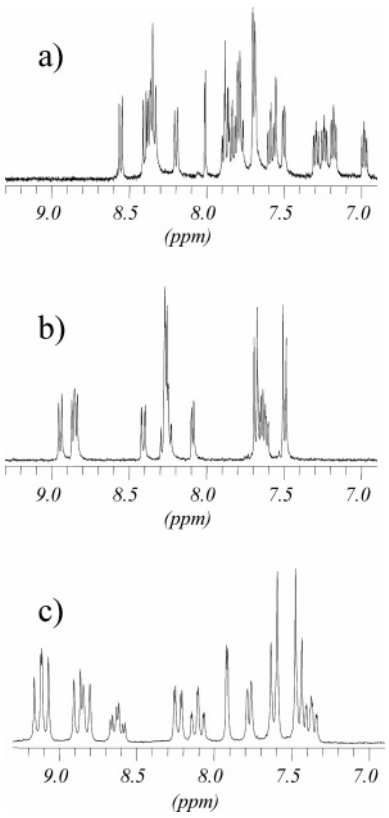

Figure 6. (a) Proton NMR of complex **1**. (b) Proton NMR of complex **3**. (c) Proton NMR of complex **6**. For the sake of clarity only the aromatic region of the spectrum are shown. All spectra have been measured in acetone-d_6 at room temperature.

prototypic examples are given in Figure 6. The spectra reveal the expected number of aromatic patterns without any overlapping. The most interesting features are given by complex **1**, whose NMR spectrum displays a splitting of the methyl and ethyl signals located in close proximity to the prochiral metal center. When the distance between the chiral Ru-center and the bodipy core such as in **2** is increased, this splitting is no longer observed. The absence of chirality in the case of the Ru−terpy

center such as in **4** also resulted in the absence of the methyl and ethyl splitting. As might be expected in the case of complexes **2** and **5**, the complexation of, respectively, the bipyridine and terpyridine fragments resulted in an upfield shift of one of the doublet of the AB quartet by ca. 0.2 ppm. The second doublet belonging to the protons in close proximity to the bodipy core is not affected. It is interesting to note that when two bodipy groups are present on the ligands, the proton NMR spectra remain remarkably symmetric, probably due to the presence of a C_2 axis bisecting the central bipyridine fragment in the case of **3** and the central pyridine ring of the terpyridine moiety in the case of **6**.

It is worth noting that all complexes display well-resolved carbon NMR spectra, but the most interesting features rely on the sp-carbons, which are well resolved as singlets at 96.4 and 86.0 ppm for complex **2** and at 96.7 and 88.4 ppm for complex **5**. In particular, by complexation of the free ligands with the metal center, the sp-carbon in close proximity with the chelating bipyridine or terpyridine is the most affected and upfield shifted by ca. 4 ppm compared to the complexed ligands.

FT-IR confirms that complexation of the free donor site by a cationic Ru center induces a significant shift of the $\nu_{C\equiv C}$ stretching vibration from the 2200−2210 cm^{-1} range in the free ligand to the 2217−2223 cm^{-1} range in the complexes. No change in the ν_{B-F} stretching frequency around 1115 cm^{-1} is found by complexation.

Finally, all complexes analyzed by electrospray mass spectroscopy gave an intense molecular peak with the expected isotopic profile corresponding to the loss of one PF_6^- counteranion. Also present is a weaker peak, corresponding to a doubly charged species, likely formed by the release of both PF_6^- anions.

Absorption Spectra. The UV absorption bands of **1**−**6** (Table 1, Figures 2−4) can be assigned to spin-allowed ligand-centered (LC) transitions. In particular, the bands within the 270−300 nm range should receive a dominant contribution from $\pi-\pi^*$ transitions involving the polypyridine moieties,[18,24] whereas the weak absorption around 360 nm is attributed to $\pi-\pi^*$ transitions involving the pyrromethene−BF_2 dyes.[25] Absorption bands in the visible region are expected to include contributions from spin-allowed metal-to-ligand charge-transfer (MLCT) transitions. Actually, such transitions contribute to the absorption feautures in the region 430−510 nm (Table 1, Figures 2−4). Finally, the narrow bands that maximize around 530 nm are assigned to the lowest-energy spin-allowed $\pi-\pi^*$ transitions involving the bodipy moieties.[21] To further confirm our attribution, it can be noted that the molar absorbance of the about-530 nm band in the various compounds strongly depends on the number of appended bodipy subunits (Table 1).

Redox Behavior. *Oxidation Processes.* All the new metal complexes undergo two reversible oxidation processes in the potential window examined (+1.80/−2.00 V vs SCE). On the basis of the potentials of the oxidation processes exhibited by the free ligands and by the model compounds $[Ru(bpy)_3]^{2+}$ and $[Ru(terpy)_2]^{2+}$ (see Table 2), the process occurring around +1.00 V can be attributed to the oxidation of the bodipy subunit(s) and the one occurring at more positive potentials to the metal-centered oxidation. Interestingly, the first oxidation process of **3** and **6** involves two electrons: this is in full agreement with the above attribution, because these complexes bear *two* bodipy subunits, which evidently behave independently of one another. It also can be noted that the oxidation potentials of bodipy subunits connected to the metal-coordinated polypyridine moiety via a phenylethynyl group (i.e., **2**, **3**, **6**) are less positive than those of the bodipy subunits of **1** and **4**, which do not contain phenylethynyl linkages (Table 2). This suggests that the phenylethynyl group can stabilize the radical cation formed upon oxidation, making the oxidation process easier.[26]

Finally, it is noteworthy that the metal-centered oxidation in **1**−**6** occurs in all the cases at more positive potentials than in the model compounds $[Ru(bpy)_3]^{2+}$ and $[Ru(terpy)_2]^{2+}$ (see Table 2). This effect can be attributed to the interaction between the two types of redox-active sites (the bodipy- and metal-centered ones) present in each complex. Such an interaction is probably due to a combination of Coulombic and electronic contributions. Indeed, the shift of the metal-centered oxidation potential to more positive values compared to the corresponding model compound (i.e., $[Ru(bpy)_3]^{2+}$ for **1**−**3**; $[Ru(terpy)_2]^{2+}$ for **4**−**6**) is somewhat larger for **1** (130 mV) and **4** (110 mV), where there is a direct connection between the two redox-active sites, compared to **2** (110 mV) and **5** (40 mV), which contain a phenylethynyl spacer (Table 2). Obviously, the larger positive shifts in the two series of complexes based on bidentate and tridentate polypyridine ligands are exhibited by the potentials of the metal-centered oxidation processes of **3** (160 mV) and **6** (140 mV); in these metal complexes there are *two* bodipy subunits per *one* metal center.

Reduction Processes. Even for the attribution of the various reduction processes of **1**−**6** to specific components, a comparison with the reduction processes of the free ligands **L1**−**L6** and of the model compounds $[Ru(bpy)_3]^{2+}$ and $[Ru(terpy)_2]^2$ is quite useful (see Table 2). From such a comparison, it can be noted that the first reduction process of each compounds of the **1**−**6** series takes place at less negative potentials compared to the first reduction of its own corresponding isolated parent. This indicates that a nonnegligible interaction takes place between the bodipy-centered and the metal complexes (i.e., the polypyridine-centered) reduction sites. A good hint for the attribution of the various processes comes from the bielectronic nature of the second reduction process of **5** and **6** (Table 2, Figure 5). Both these complexes indeed bear two bodipy centers that, as indicated by the oxidation behavior (see above), are noninteracting one another. As a consequence, they are expected to be reduced simultaneously. Such a line of reasoning allows us to identify the bielectronic reduction process of **3** at −1.35 V and of **6** at −1.33 V as bodipy-centered processes. As a consequence, the other reduction processes of the two complexes are straightforwardly attributed to the one-electron successive reductions of the polypyridine ligands.

On the basis of the above-mentioned attributions for the reduction processes of **3** and **6**, the reduction processes of the other metal complexes can be assigned. In general, the process occurring at a potential close to −1.35 V is assigned to the bodipy subunits, and the other processes to the polypyridine ligands. The reduction patterns of complexes **2** and **6** need further clarifications: for complex **6**, the last reduction process at −1.60 V is probably due to the second reduction of a terpy-like ligand, in particular of the ligand whose first reduction occurs at −1.06 V. However, the potential separation between such potentials, 540 mV, cannot be related to the electron pairing energy in coordinated polypyridine ligands.[27,28] As far as complex **2** is concerned, the reduction process at −1.37 V involves two electrons: we suggest that the two electrons are not added to two noninteracting, identical sites, but reduction of bodipy and of one bpy ligand casually occurs at the same potential.

As far as the origin of the shift of the reduction potential of the first, polypyridine-centered reduction process of **1**−**6**

compared to the first reduction of the model metal complexes (Table 2) is concerned, it is probably due to the acceptor ability of the bodipy ligands, which stabilizes the LUMO of the metal-based subunits. This effect obviously is more effective on the polypyridine ligands directly connected to the bodipy moieties, so these ligands should also be the ones involved in the first reduction process in all the complexes, with the other, peripheral polypyridine ligands being the sites of the successive reductions.

Photophysical Properties. *Luminescence Spectra and Lifetimes.* Bodipy dyes are well-known and efficient fluorophores.[6−15] Ru(II) polypyridine complexes, on the other hand, are probably the most investigated inorganic luminophores.[18,30] However, compounds **1**−**6**, made of Ru(II) polypyridine and bodipy subunits, do not show any luminescence in fluid solution at room temperature (Table 1): in particular, both the fluorescence of the **L1**−**L6** free ligands and the (formal) phosphorescence of Ru(II) polypyridine complexes are absent in these experimental conditions. By using a nanosecond transient absorption spectra apparatus, anyway, we found that in all the metal complexes a relatively long-lived (microsecond time scale) excited state was formed (see later).

At 77 K in rigid matrix, fluorescence of the bodipy subunits is present also in the metal complexes, although with lifetimes slightly reduced compared to those of the corresponding free ligands (see Table 1). The fluorescence energy was roughly constant on passing from the free ligands to the metal complexes, so indicating that the effect of the metal-based chromophores on the energy levels of the bodipy subunits is small. The long-lived emission at about 770 nm exhibited by **4**−**6** cannot be the ^{3}MLCT emission, on the basis of the energy and lifetime (see Table 1). From model species, in fact, ^{3}MLCT emission for **1**−**6** at 77 K would be expected at wavelengths shorter than 720 nm and with a lifetime in the microsecond time scale.[18,29,30] The millisecond lifetime of the emission strongly indicates that its origin is an organic triplet state, so it can be safely assigned to phosphorescence originating from the bodipy-centered $^3\pi\pi^*$ level.

From the literature data[18c,29,30] and the experimental results, the energy level diagram shown in Figure 7 can be drawn (in such a diagram, only the lowest energy states are represented). On the basis of the experimental results, the lowest-lying ^{1}MLCT state should be located between 2.75 and 2.50 eV (the energy is approximated from the spin-allowed MLCT bands in the absorption spectra of **1**−**6**, also in agreement with literature data). The lowest-lying bodipy-centered $^1\pi-\pi^*$ should be in a rather narrow range between 2.32 and 2.28 eV (energy estimated from literature data[18,29,30] and the fluorescence spectra reported here). Still from literature data[18c,29] and taking into account the structures of **1**−**6**, the lowest-energy ^{3}MLCT states of **1**−**6** are located between 2.00 and 1.72 eV. Finally, the lowest-energy level in all the complexes should be a bodipy-centered $^3\pi-\pi^*$ state, as also indicated by nanosecond transient absorption data (see later); taking into account the 77 K phosphorescence of **4**−**6**, this state should approximately lie between 1.65 and 1.55 eV in this series of metal complexes.

The scheme in Figure 7 accounts for the quenching of MLCT emission in **1**−**6**: the triplet MLCT state indeed would decay to the bodipy-centered $^3\pi-\pi^*$ level by intercomponent energy transfer, and such a process should be effective both at 77 K and at room temperature. The bodipy fluorescence quenching is less straightforward to explain: in fact, such a fluorescence in **1**−**6** could be quenched by an intersystem crossing process that should be enhanced (compared to the free ligands, where it is poorly efficient) in **1**−**6** by the presence of the heavy metal centers. Intersystem crossing is indeed an effective decay pathway, as indicated by the 77 K luminescence properties of **4**−**6** (see discussion later). However, if enhanced intersystem crossing was the main reason for bodipy fluorescence quenching in **1**−**6** at room temperature, fluorescence should be quenched (totally or at least largely) also at 77 K. On the contrary, in this latter experimental condition such a quenching process does not appear to be so efficient (according to the moderate shortening of the 77 K fluorescence lifetimes of **1**−**6** compared to those of the corresponding free ligands, see Table 1) to justify the total absence of bodipy-centered fluorescence at room temperature. The ^{3}MLCT level can hardly play the role of intermediate for the intersystem crossing process, because bodipy-centered fluorescence cannot be fastly quenched via intercomponent energy transfer to populate the ^{3}MLCT level: in fact, the Förster equation for Coulombic energy transfer[31] yields values lower than 1×10^6 s^{-1} for this process in **1**−**6**, mainly due to the negligible absorption of the metal subunits at $\lambda > 510$ nm, and these values cannot compete with intrinsic deactivation of the

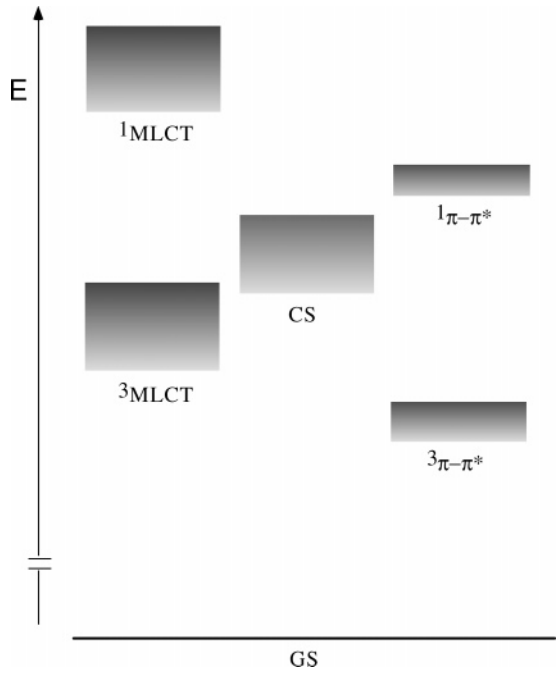

Figure 7. Estimated energy level diagram of **1**−**6**. For each excited state, a range of energy is indicated to include all the species (see text). On the left are represented metal-based levels, whereas bodipy-centered levels are represented on the right. In the middle is shown the charge-separated state (CS), which is a multicomponent (supramolecular) state. GS is the ground state. The deactivation processes between the states are discussed in the main text.

TABLE 3: Driving Force ΔG_{CS} and "Lifetime" τ_{CS} of the Quenching of the bodipy-Centered Singlet State at Room Temperature Leading to Charge Separation (CS) and "Lifetime" τ_{CR} of the Charge Recombination Processes Leading to bodipy-Centered Triplet State (See Text)

compound	ΔG_{CS}, eV	τ_{CS}, ps	τ_{CR}, ps
1	−0.16	6[a]	
2	−0.13	30	200
3	−0.31	3	96
4	−0.21	2.5	70
5	−0.17	8	40
6	−0.25	11	100

[a] This figure most likely refers to direct intersystem crossing (see text).

bodipy singlet. Electron exchange (Dexter)[32] energy transfer appears also unlikely, because it would be a spin-forbidden process.[33]

Another process (requiring the presence of another excited state) can be considered to account for the quenching of the bodipy-centered fluorescence in **1**−**6** at room temperature and could have the effect of mediating the intersystem crossing between bodipy-centered singlet and triplet excited states: such a process is typical of the multicomponent nature of the new **1**−**6** complexes and involves a charge-separated state, produced from the bodipy-centered $^1\pi-\pi^*$ level by oxidative electron transfer to the metal-based chromophore(s). Actually, in all the complexes, by using the eq 1 for calculating the driving force of the process,[2,34] the oxidative electron transfer is thermodynamically allowed. Driving forces in the various cases are between −0.13 and −0.31 eV and are collected in Table 3.

$$\Delta G = e(^*E_{ox(bodipy)} - E_{red(Ru)}) \quad (1)$$

The moderate exoergonicity of the oxidative electron-transfer process could explain why such a process is efficient at room temperature, whereas it is less efficient at 77 K in rigid matrix, where bodipy fluorescence takes place (except for **1**). Moderately exoergonic electron transfer processes are in fact rarely efficient at low temperature in rigid matrix, because of the presence of nuclear barriers.[2,35] At 77 K, the oxidative electron transfer from the bodipy-centered $^1\pi-\pi^*$ level would therefore be inefficient, allowing for bodipy-centered fluorescence to compete with direct intersystem crossing to the bodipy-centered triplet.

The room temperature decay process warrants some other comments: from the estimation given above of the bodipy-centered $^1\pi-\pi^*$ level, the charge-separated states should lie between 2.19 and 1.97 eV. Therefore, back electron transfer (a charge recombination process) from the charge-separated state to directly produce the ground state would deeply be in the Marcus inverted region and should be rather slow.[1,2] Charge recombination to produce the triplet bodipy-centered $\pi-\pi^*$ level could be preferred, and indeed this latter process seems to dominate the decay of **1**−**6**, as testified by transient absorption data (see later). It could be curiously noted that for **4**−**6**, which exhibit luminescence from such a triplet state at 77 K, the charge recombination from the charge-separated state and successive emission is equivalent to a chemiluminescent process.

Finally, we would like to highlight that **4**−**6** are the first species, to the best of our knowledge, displaying phosphorescence from bodipy subunits. In fact, although these latter chromophores have been extensively studied,[7−17] radiative deactivation from the triplet state has never been reported. We propose that the 77 K phosphorescence of the bodipy subunits in **4**−**6** is due to the presence of the heavy ruthenium metal, which would allow intensity to be stolen from spin-allowed radiative decays by enhanced spin−orbit coupling. In particular, it is probably the interaction between the bodipy $^3\pi\pi^*$ state and the closely lying metal-based ^{3}MLCT level (for which luminescence decay is highly efficient at 77 K) that provides a channel to gain bodipy-based phosphorescence in the present systems. Why bodipy phosphorescence is an effective decay process in **4**−**6**, containing terpy-type ligands, and apparently is not effective in **1**−**3**, based on bpy-type ligands, has not been clarified.

Transient Absorption Spectroscopy. To further clarify the photophysical properties of **1**−**6**, we performed room temperature transient absorption spectroscopy of the complexes as well as of the free ligands. We employed both a nanosecond flash-photolysis apparatus and a femtosecond pump−probe equipment. Excitation wavelength was 450 nm for the femtosecond apparatus and 352 nm for the nanosecond equipment.[36] The transient absorption spectra of the free ligands **L1**−**L6**, which only have been investigated by the nanosecond apparatus,[36] are very similar one another, and display a single feature, which is bleaching of the absorption band at about 525 nm. Recovery of the bleaching cannot be measured, because it is on the same time scale of laser pulse (8 ns), but such a result is in agreement with the luminescence lifetime data and suggests that the transient absorption spectra actually correspond to the singlet bodipy-based fluorescent states. Recovery on the nanosecond time scale is more than 90% efficient in all the cases, but it is not complete. This suggests that some triplet is formed, although with poor efficiency.

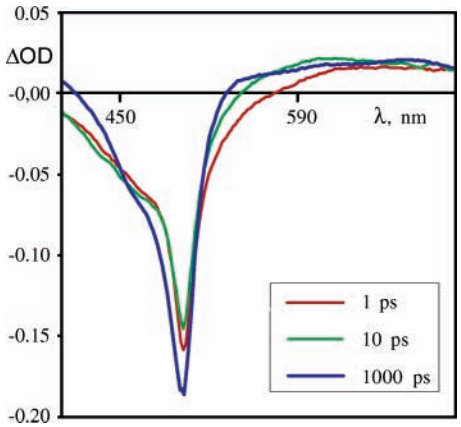

Figure 8. Femtosecond transient absorption spectra of **5** in acetonitrile at room temperature.

The transient spectra and decays are much more complicated for the metal complexes **1**−**6**. These species (but **1**) displaced qualitatively similar spectral and decay evolutions. After 1 ps from laser pulse, a typical spectrum (see Figure 8 for complex **5**) shows a strong bleach in the 530 nm region and a comparably weak and broad absorption at wavelength longer than 570 nm. Interestingly, although the excitation wavelength is 450 nm, which is mainly centered in the MLCT band, the bleach of the singlet MLCT band is less pronounced compared to that of the bodipy-centered singlet state, even considering the different molar absorbance values (cfr. Figures 3 and 8). The transient spectrum evolves, with rate constants between 3 and 15 ps for the various complexes, showing a slight recovery of the 530 nm bleach and the rising of a strong absorption in the 540−700 nm region. This relatively fast process is followed by a slower process (rate constants between 30 and 200 ps), leading to an increased bleach at 530 nm and to modification of the absorption profiles in the 540−700 nm region (Figure 8). The transient spectra finally obtained for all the complexes are constant on the nanosecond time scale, and indeed their decays can be appreciated only with a slower apparatus, which show that the decay rate constants are in the tens of microseconds time scale (Table 1 and Figure S1, Supporting Information). The exception here is complex **1**: for this species, the spectrum recorded after 1 ps from laser pulse decays directly to the final transient spectrum.

The transient absorption spectroscopy can be rationalized on looking at the energy level diagram in Figure 7: laser excitation produces ^{1}MLCT and the bodipy-centered $^1\pi-\pi^*$ levels. Several indications are in favor of an ultrafast transfer of energy from ^{1}MLCT to bodipy-centered levels as the dominant deactivation route of the ^{1}MLCT state,[37] so we can assume that after 1 ps

the only singlet state in which excitation resides is the $^1\pi-\pi^*$ level. This state at room temperature deactivates by oxidative electron transfer to the charge-separated state. Such a process is the first process evidenced by transient absorption spectroscopy, which is the process occurring in the 3−15 ps time scale. The slower, successive process (time scale 30−200 ps) is assigned to the charge recombination process leading to the bodipy-centered $^3\pi-\pi^*$ level. This state should be long-lived, as expected for an organic triplet state, so justifying the microsecond time scale of the decay of the "final" transient spectra (see Table 1). Table 3 collects rate constants and calculated driving forces for the various processes of the **1**−**6** series.

As mentioned above, **1** exhibits a single fast decay process. In fact, the initially formed transient spectrum evolves to the one assigned to the triplet state with no evidence of formation of the intermediate charge-separated species. Once formed, this "final" transient spectrum, which is very close to the "final" transient spectra of **2**−**6**, also decays to the ground state in the microsecond regime. Furthermore, **1** also does not exhibit any fluorescence at 77 K. This could suggest that (i) the charge recombination process is extremely fast for this species and the charge-separated species cannot accumulate, (ii) the nuclear barriers for charge separation and charge recombination processes in **1** are significantly smaller than for **2**−**5**, so allowing efficient electron-transfer quenching of the bodipy $^1\pi-\pi^*$ level—and successive formation of the corresponding triplet state—even at 77 K, and (iii) intersystem crossing between bodipy-centered singlet and triplet states could be faster than in the other species (in this case, the 6 ps decay of the initially formed $^1\pi-\pi^*$ level at room temperature could just be due to the direct intersystem crossing populating the corresponding triplet state, rather than the oxidative electron-transfer populating the charge-separated state). Case (i) alone cannot justify the absence of fluorescence at 77 K, so it should be at least combined with one of the other reasons. Although it can be noted that **1** is the species characterized by the smaller distance between the bodipy subunit and the metal center in the series (slightly smaller even in comparison with **4**), this fact can have an effect both on the intersystem crossing rate (proximity of the heavy Ru center can affect the extent of the intersystem crossing) and on electron transfer nuclear barrier (mainly acting on the reorganization energy). Therefore, we have no simple way to discriminate between the above hypotheses and some of the properties of **1** remain unclear.

Conclusions

Six new multichromophoric species (**1**−**6**) containing Ru(II) polypyridine and bodipy subunits have been prepared and their absorption spectra, luminescence properties (both at room temperature in fluid solution and at 77 K in rigid matrix), and redox properties have been investigated. Transient absorption spectroscopy have also been performed at room temperature. Absorption spectra and redox behavior indicate the supramolecular nature of the multichromophoric assemblies, allowing us to assign the various absorption features and the several redox processes to specific subunits. Despite the good luminescence properties of the separated components, **1**−**6** do not exhibit any luminescence at room temperature. However, transient absorption spectroscopy evidences that for all of them a long-lived (microsecond time scale) excited state is formed, which is identified as the bodipy-based triplet state. It is proposed that such a triplet state is formed in most cases by the intervening of a charge-separated level from the bodipy-based $^1\pi-\pi^*$ state. At 77 K, all the complexes except complex **1**, exhibit the bodipy-based fluorescence, although with a slightly shortened lifetime compared to the corresponding free ligand(s), and **4**−**6** also exhibit a phosphorescence assigned to the bodipy subunits. To the best of our knowledge, phosphorescence of bodipy species had never been reported in the literature:[20] in the present cases we propose that it can be an effective decay process thanks to the presence of the ruthenium heavy atom and of the closely lying ^{3}MLCT state of the Ru(terpy)$_2$-type subunits.

Experimental Section

Materials and Methods. Absorption spectra were recorded with a JASCO 560 spectrophotometer. Luminescence spectra were performed with a Spex-Jobin Yvon Fluoromax-P spectrofluorometer equipped with a Hamamatsu R3896 photomultiplier, and were corrected for photomultiplier response using a program purchased with the fluorometer. Emission lifetimes were measured with an Edinburgh OB-900 single-photon counting spectrometer equipped with a Hamamatsu PLP-2 laser diode (pulse width at 408 nm, 59 ps). Luminescence quantum yields have been calculated by using the optically dilute method.[41] Nanosecond transient absorption spectra and lifetimes were measured with an Applied Photophysics laser flash photolysis apparatus, with frequency doubled, (532 nm, 330 mJ) or tripled, (355 nm, 160 mJ) Surelite Continuum II Nd:YAG laser (halfwidth 4−6 ns), photomultiplier (Hamamatsu R928) signals were processed by means of a LeCroy 9360 (600 MHz, 5 Gs/s) digital oscilloscope. Femtosecond time-resolved experiments were performed using a pump−probe spectrometer based on the Spectra-Physics Hurricane Ti:sapphire system as the laser source. The pump pulse was generated either by a frequency doubler (400 nm) or with a Spectra Physics 800 OPA (tunable in the range 488−600 nm). The probe pulse was obtained by continuum generation on a sapphire plate (useful spectral range, 450−800 nm). Effective time resolution ca. 300 fs, temporal chirp over the white-light 450−750 nm range ca. 200 fs, temporal window of the optical delay stage 0−1000 ps.

The 400.1, 200.1 (^{1}H) and 100.6, 50.6 (^{13}C) NMR spectra were recorded at room temperature using residual proton or carbon signals, respectively, of the deuterated solvents as internal references. A fast-atom bombardment ZAB-HF-VB-analytical apparatus in positive mode was used with a *m*-nitrobenzyl alcohol (*m*-NBA) as the matrix. FT-IR spectra were recorded on the neat liquids or as thin films, prepared with a drop of dichloromethane and evaporated to dryness on KBr pellets. Chromatographic purification was conducted using 40−63 μm silica gel or aluminum oxide 90 standardized. Thin-layer chromatography (TLC) was performed on silica gel or aluminum oxide plates coated with fluorescent indicator. All mixtures of solvents are given in v/v ratio. The experimental procedures for each reaction were tested several times to optimize conditions.

Electrochemical studies employed cyclic voltammetry with a conventional three-electrode system using a BAS CV-50W voltammetric analyzer equipped with a Pt microdisk (2 mm^2) working electrode and a platinum wire counter-electrode. Ferrocene was used as an internal standard and was calibrated against a saturated calomel reference electrode (SCE) separated from the electrolysis cell by a glass frit presoaked with electrolyte solution. Solutions contained the electro-active substrate (ca. 5.0×10^{-3} M) in deoxygenated and anhydrous nitrogen with tetra-*n*-butylammonium hexafluorophosphate (0.1 M) as supporting electrolyte. The quoted half-wave potentials were reproducible within ±10 mV.

Experimental uncertainties are as follows: absorption maxima, ±2 nm; molar absorption coefficient, 10%; emission maxima, ±5 nm; excited-state lifetimes, 10%; luminescence quantum yields, 20%.

Synthesis and Characterization of Complexes 1−6. *General Procedure for the Preparation of the Ruthenium Bipyridine Complexes.* In a Schlenk flask, a stirred dichloromethane solution containing one equivalent of the ligand was treated with an ethanol solution containing one equivalent of $[Ru(bipy)_2]Cl_2 \cdot 2H_2O$ and heated at 60 °C overnight. After complete consumption of starting material (determined by TLC), an aqueous solution (5 equiv) of KPF_6 was added, the organic solvent was then removed under vacuum. The precipitates were washed by centrifugation with water until the solution was colorless. The target complexes were purified by chromatography on alumina eluting with dichloromethane using a gradient of methanol. The pure red complexes were obtained by double recrystallization in acetone/hexane.

General Procedure for the Preparation of the Ruthenium Terpyridine Complexes. A stirred solution of *cis*-$[Ru(terpy)(DMSO)Cl_2]$ and $AgBF_4$ (2.2 equiv respectively) in argon degassed methanol was heated at 80 °C for 6 h in a Schlenk round-bottom flask. After cooling to ambient temperature, the precipitate (AgCl) was separated by filtration under argon over cotton-wool and the deep-red solution quantitatively transferred via cannula to a methanol (20 mL) solution containing the corresponding ligand (100 mg, 1 equiv). The progression of the complexation reaction was followed by thin-layer chromatography (TLC), which clearly showed the consumption of the free ligand and the formation of the desired complexes. After a 15 h, the clear red solution was cooled to ambient temperature and filtered over Celite and an aqueous solution (2 mL) of NH_4PF_6 (10 equiv) was added. Slow evaporation of the organic solvent led to the precipitation of a deep-red solid, which is recovered by centrifugation and washed three times with water (3 × 20 mL) and diethyl ether (2 × 10 mL). The crude material was dried under high vacuum and ultimately purified by chromatography over alumina using dichloromethane as solvent and an increasing gradient of methanol (3−10%). Finally, the purified complexes were recrystallized from a 1/1 mixture of acetonitrile/toluene affording the analytically pure complexes.

*Ruthenium Bis(2,2′-bipyridine)[4,4-difluoro-8-(5″-methyl-2′,2″-bipyridin-5′-y)-1,3,5,7-tetramethyl-2,6-diethyl-4-bora-3a,4a-diaza-s-indacene] Bis(hexafluorophosphate) (**1**).* Isolated yield: 42%. ^{1}H NMR (400.1 MHz, acetone-d_6): δ 0.64 (s, 3H), 0.97 (t, 3H, ^3J = 7.0 Hz), 1.05 (t, 3H, ^3J = 7.0 Hz), 1.74 (s, 3H), 2.19 (q, 2H, ^3J = 7.0 Hz), 2.24 (s, 3H), 2.34 (q, 2H, ^3J = 7.0 Hz), 2.39 (s, 3H), 2.38 (s, 3H), 6.98 (td, 1H, ^3J = 6.2 Hz, ^4J = 1.0 Hz), 7.18 (td, 1H, ^3J = 6.5 Hz, ^4J = 1.2 Hz), 7.24 (td, 1H, ^3J = 6.5 Hz, ^4J = 1.2 Hz), 7.29 (td, 2H, ^3J = 6.5 Hz, ^4J = 1.2 Hz), 7.49 (d, 1H, ^3J = 5.4 Hz), 7.55 (s, 1H), 7.59 (td, 1H, ^3J = 7.3 Hz, ^4J = 1.3 Hz), 7.70 (d, 2H, ^3J = 5.1 Hz), 7.80 (q, 2H, ^3J = 6.5 Hz, ^4J = 1.2 Hz), 7.88 (m, 2H), 8.00 (d, 1H, ^4J = 1.3 Hz), 8.19 (d, 1H, ^3J = 7.3 Hz), 8.36 (m, 5H), 8.55 (d, 1H, ^3J = 7.3 Hz). ^{13}C{^{1}H} NMR (100.6 MHz, acetone-d_6): δ 11.6, 12.6, 12.7, 13.6, 14.9, 15.0, 17.3, 17.4, 125.2, 125.3, 125.4, 125.6, 125.7, 128.6, 128.7, 128.8, 128.8, 134.0, 134.4, 135.8, 138.8, 139.1, 139.2, 139.3, 139.5, 139.7, 140.3, 152.0, 152.7, 152.8, 152.8, 152.9, 152.9, 155.0, 155.6, 156.0, 157.9, 158.0, 158.3, 158.4, 159.0.

UV−vis (CH_3CN): λ_{max} (ϵ, M^{-1} cm^{-1}) 532 nm (36 100). See other data in Table 1.

IR (KBr), cm^{-1}: 3083 (m), 2967 (m), 2926 (m), 2870 (m), 1711 (m), 1603 (m), 1547 (s), 1466 (s), 1446 (s), 1320 (s), 1272 (m), 1191 (s), 1067 (m), 978 (s), 839 (s), 763 (m), 730 (s).

ES−MS in acetonitrile at V_c = 100 V, *m*/*z* (%) [peak attribution]: 1031.2 (100) $[M - PF_6]^+$, 443.1 (40) $[M - 2PF_6]^{2+}$.

Anal. Calcd for $C_{48}H_{47}N_8BRuP_2F_{14}$: C, 49.03; H, 4.03; N, 9.53. Found: C, 48.77; H, 3.83; N, 9.41.

*Ruthenium Bis(2,2′-bipyridine)(5-{ethynylphenyl-4″-[4‴,4‴-difluoro-8‴-(1‴,3‴,5‴,7‴-tetramethyl-2‴,6‴-diethyl-4‴-bora-3‴a,4‴a-diaza-s-indacene)]}-2,2′-bipyridine) Bis(hexafluorophosphate) (**2**).* Isolated yield: 86%. ^{1}H NMR (200.1 MHz, acetone-d_6): δ 0.98 (t, 6H, ^3J = 7.5 Hz), 1.33 (s, 6H), 2.34 (q, 4H, ^3J = 7.5 Hz), 2.49 (s, 6H), 7.48 (d, 2H, ^3J = 8.5 Hz), 7.57−7.60 (9 lines m, 4H), 7.58 (ABsys, 4H, J_{AB} = 8.4 Hz, $\nu_0\delta$ = 76.3 Hz), 8.02−8.12 (10 lines m, 4H), 8.11−8.27 (m, 6H), 8.37 (dd, 1H, ^3J = 8.5 Hz, ^4J = 2.0 Hz), 8.82−8.90 (m, 6H). ^{13}C-{^{1}H} NMR (50.1 MHz, acetone-d_6): δ 12.1, 12.6, 14.9, 17.5, 86.0 (C≡C), 96.4 (C≡C), 123.0, 124.5, 125.0, 125.4, 125.4, 125.5, 125.5, 125.9, 128.8, 128.9, 129.0, 130.1, 138.1, 138.8, 139.5, 141.0, 152.6, 152.8, 152.9, 153.1, 154.4, 154.9, 157.5, 157.7, 158.1, 158.2.

IR (KBr), cm^{-1}: 3118 (m), 3083 (m), 2962 (m), 2926 (m), 2870 (m), 2222 ($\nu_{C\equiv C}$), 1714 (m), 1603 (m), 1537 (s), 1464 (s), 1317 (s), 1272 (m), 1241 (m), 1191 (s), 1160 (m), 1064 (m), 978 (s), 837 (s), 761 (m), 731 (s).

UV−vis (CH_3CN, 23 °C): λ_{max} (ϵ, M^{-1} cm^{-1}) 523 nm (61 340). See other data in Table 1.

ES−MS in acetonitrile at V_c = 100 V, *m*/*z* (%) [peak attribution]: 1117.2 (100) $[M - PF_6]^+$, 486.2 (20) $[M - 2PF_6]^{2+}$.

Anal. Calcd for $C_{55}H_{49}BRuP_2F_{14}N_8$: C, 52.35; H, 3.91; N, 8.88. Found: C, 52.17; H, 3.73; N, 9.04.

*Ruthenium Bis(2,2′-bipyridine)(5,5′-{bis-ethynylphenyl-4″-[4‴,4‴-difluoro-8‴-(1‴,3‴,5‴,7‴-tetramethyl-2‴,6‴-diethyl-4‴-bora-3‴a,4‴a-diaza-s-indacene)]}-2,2′-bipyridine) Bis-(hexafluorophosphate) (**3**).* Isolated yield: 75%. ^{1}H NMR (400.1 MHz, acetone-d_6): δ 0.98 (t, 12H, ^3J = 7.5 Hz), 1.33 (s, 12H), 2.34 (q, 8H, ^3J = 7.5 Hz), 2.50 (s, 12H), 7.59 (ABsys, 8H, J_{AB} = 8.5 Hz, $\nu_0\delta$ = 76.5 Hz), 7.64 (8 lines m, 4H), 8.08 (d, 2H, ^3J = 5.0 Hz), 8.27 (11 lines m, 8H), 8.40 (dd, 2H, ^3J = 8.5 Hz, ^4J = 1.5 Hz), 8.85 (lt, 4H, ^3J = 7.5 Hz), 8.94 (d, 2H, ^3J = 8.5 Hz). ^{13}C{^{1}H} NMR (100.6 MHz, acetone-d_6): δ 12.1 (CH_3), 12.7 (CH_3), 14.9 (CH_3), 17.5 (CH_2), 86.1, 96.8, 123.0, 124.7, 125.5, 125.6, 128.9, 128.9, 130.2, 131.1, 133.3, 133.9, 138.2, 138.8, 139.2, 140.2, 141.0, 152.8, 153.2, 154.6, 154.9, 156.9, 158.2, 158.3.

UV−vis (CH_3CN, 23 °C): λ_{max} (ϵ, M^{-1} cm^{-1}) 523 nm (86 700). See other data in Table 1.

IR (KBr), cm^{-1}: 2963 (m), 2928 (m), 2864 (m), 2223 ($\nu_{C\equiv C}$), 1723 (m), 1604 (m), 1538 (s), 1473 (s), 1446 (m), 1320 (s), 1270 (m), 1192 (s), 1160 (m), 1115 (m), 1066 (m), 977 (s), 840 (s), 76 (m).

ES−MS in acetonitrile at V_c = 100 V, *m*/*z* (%) [peak attribution]: 1519.3 (100) $[M - PF_6]^+$, 687.2 (30) $[M - 2PF_6]^{2+}$, 668.2 (<5) $[M - 2PF_6 - 2F]^{2+}$.

Anal. Calcd for $C_{80}H_{74}B_2F_{16}N_{10}RuP_2$: C, 57.74; H, 4.48; N, 8.42. Found: C, 57.48; H, 4.23; N, 8.18.

*Ruthenium (2,2′:6′,2″-Terpyridine)[4,4-difluoro-8-(2′:2″;6″:2‴terpyridin-4″-yl)-1,3,5,7-tetramethyl-2,4-diethyl-4-bora-3a,4a-diaza-s-indacene] Bis(hexafluorophosphate) (**4**).* Isolated yield: 63%. ^{1}H NMR (200.1 MHz, acetone-d_6): δ 1.05 (t, 6H, ^3J = 7.3 Hz), 1.93 (s, 6H), 2.46 (q, 4H, ^3J = 7.3 Hz), 2.62 (s, 6H), 7.38 (m, 5H), 7.57 (d, 2H, ^3J = 5.1 Hz), 7.77 (d, 2H, ^3J

= 5.1 Hz), 8.10 (t, 2H, ^3J = 8.0 Hz), 8.62 (t, 2H, ^3J = 8.0 Hz), 8.84 (d, 2H, ^3J = 8.0 Hz), 8.95 (d, 2H, ^3J = 8.0 Hz), 9.11 (d, 2H, ^3J = 8.0 Hz), 9.28 (s, 2H). $^{13}C\{^1H\}$ NMR (50.6 MHz, acetone-d_6): δ 12.9 (CH_3), 13.3 (CH_3), 15.1 (CH_3), 17.5 (CH_2), 125.0, 125.1, 125.6, 125.7, 126.4, 126.5, 128.6, 129.1, 139.1, 152.8, 153.5, 153.8, 156.2, 157.7, 158.9, 159.3.

UV−vis (CH_3CN, 23 °C): λ_{max} (ϵ, M^{-1} cm^{-1}) 531 nm (24 900). See other data in Table 1.

IR (KBr), cm^{-1}: 2963 (m), 2923 (m), 2873 (m), 1713 (m), 1602 (m), 1540 (s), 1448 (s), 1387 (s), 1288 (m), 1189 (s), 1058 (m), 1028 (m), 974 (s), 838 (s), 769 (m).

ES−MS in acetonitrile at V_c = 100 V, *m*/*z* (%) [peak attribution]: 1015.2 (100) $[M - PF_6]^+$, 435.1 (20) $[M - 2PF_6]^{2+}$, 426.1 (5) $[M - 2PF_6 - F]^{2+}$.

Anal. Calcd for $C_{47}H_{43}N_8BRuP_2F_{14}$: C, 48.68; H, 3.74; N, 9.66. Found: C, 48.37; H, 3.43; N, 9.84.

*Ruthenium (2,2′:6′,2″-Terpyridine)(4′-{ethynylphenyl-4‴-[4⁗,4⁗-difluoro-8⁗-(1⁗,3⁗,5⁗,7⁗-tetramethyl-2⁗,6⁗-diethyl-4⁗-bora-3⁗a,4⁗a-diaza-s-indacene)]}-2:2′;6′:2″terpyridine) Bis(hexafluorophosphate) (**5**).* Isolated yield: 68%. ^1H NMR (200.1 MHz, acetone-d_6): δ 1.02 (t, 6H, ^3J = 7.4 Hz), 1.46 (s, 6H), 2.37 (q, 4H, ^3J = 7.4 Hz), 2.53 (s, 6H), 7.34 (9 lines m, 4H), 7.64 (5 lines m, 2H), 7.77 (5 lines m, 4H), 7.97−8.11 (m, 6H), 8.60 (6 lines m, 1H), 8.79−8.95 (8 lines m, 4H), 9.08 (4 lines m, 2H), 9.25 (d, J = 4.0 Hz, 2H). $^{13}C\{^1H\}$ NMR (50.6 MHz, acetone-d_6): δ 12.1 (CH_3), 12.7 (CH_3), 14.9 (CH_3), 17.5 (CH_2), 88.5 (C≡C), 96.8 (C≡C), 123.2, 125.6, 125.8, 125.9, 126.1, 126.3, 128.2, 128.5, 128.7, 128.9, 129.0, 130.9, 133.6, 133.7, 133.8, 134.0, 138.9, 139.3, 139.4, 139.5, 139.7, 139.9, 153.7, 153.8, 153.9, 154.0, 154.9, 156.3, 156.7, 158.8, 159.3.

UV−vis (CH_3CN, 23 °C): λ_{max} (ϵ, M^{-1} cm^{-1}) 523 nm (66 100). See other data in Table 1.

IR (KBr), cm^{-1}: 3114 (m), 3078 (m), 2967 (m), 2931 (m), 2871 (m), 2218 ($\nu_{C\equiv C}$), 1603 (m), 1537 (s), 1477 (s), 1449 (s), 1320 (s), 1272 (m), 1194 (s), 1161 (m), 1052 (m), 979 (s), 837 (s), 766 (m) cm^{-1}.

ES−MS in acetonitrile at V_c = 100 V, *m*/*z* (%) [peak attribution]: 1115.2 (100) $[M - PF_6]^+$, 485.2 (25) $[M - 2PF_6]^{2+}$, 476.0 (<10) $[M - 2PF_6 - F]^{2+}$.

Anal. Calcd for $C_{55}H_{47}N_8BRuP_2F_{14}$: C, 52.44; H, 3.76; N, 8.89. Found: C, 52.63; H, 3.97; N, 9.02.

*Ruthenium (2,2′:6′,2″-Terpyridine)(5,5″-{bis-ethynylphenyl-4‴-[4⁗,4⁗-difluoro-8⁗-(1⁗,3⁗,5⁗,7⁗-tetramethyl-2⁗,6⁗-diethyl-4⁗-bora-3⁗a,4⁗a-diaza-s-indacene)]}-2:2′;6′:2″-terpyridine) Bis(hexafluorophosphate) (**6**).* Isolated yield: 73%. ^1H NMR (200.1 MHz, acetone-d_6): δ 0.96 (t, 12H, ^3J = 7.4 Hz), 1.30 (s, 12H), 2.33 (q, 8H, ^3J = 7.4 Hz), 2.48 (s, 12H), 7.37 (td, 2H, ^3J = 6.0 Hz, ^4J = 1.1 Hz, 7.53 (AB sys, 8H, J_{AB}= 8.4 Hz, $\nu_0\delta$ = 87.9 Hz), 7.77 (d, 2H, ^3J = 4.8 Hz), 7.93 (d, 2H, ^4J = 1.4 Hz), 8.10 (td, 2H, ^3J = 7.9 Hz, ^4J = 1.4 Hz), 8.23 (dd, 2H, ^3J = 8.4 Hz, ^4J = 1.8 Hz), 8.62 (td, 2H, ^3J = 8.2 Hz, ^4J = 2.3 Hz), 8.82 (d, 2H, ^3J = 8.1 Hz), 8.88 (d, 2H, ^3J = 8.4 Hz), 9.09 (d, 2H, ^3J = 8.4 Hz), 9.14 (d, 2H, ^3J = 8.4 Hz). $^{13}C\{^1H\}$ NMR (50.6 MHz, acetone-d_6): δ = 12.1 (CH_3), 12.6 (CH_3), 14.9 (CH_3), 17.5 (CH_2), 85.7 (C≡C), 96.4 (C≡C), 122.9, 124.5, 125.0, 125.1, 125.5, 125.7, 128.7, 130.1, 131.1, 133.3, 133.9, 137.1, 137.5, 138.1, 138.8, 139.4, 140.2, 141.3, 153.8, 154.9, 155.3, 156.2, 156.7, 158.4, 159.5.

UV−vis (CH_3CN, 23 °C): λ_{max} (ϵ, M^{-1} cm^{-1}) 523 nm (89 600). See other data in Table 1.

IR (KBr), cm^{-1}: 3113 (m), 3073 (m), 2962 (m), 2926 (m), 2871 (m), 2223 ($\nu_{C\equiv C}$), 1717 (m), 1598 (m), 1537 (s), 1477 (s), 1449 (m), 1320 (s), 1276 (m), 1194 (s), 1160 (m), 1115 (s), 1067 (m), 979 (s), 834 (s), 761 (m) cm^{-1}.

ES−MS in acetonitrile at V_c = 100 V, *m*/*z* (%) [peak attribution]: 1517.3 (100) $[M - PF_6]^+$, 686.2 (35) $[M - 2PF_6]^{2+}$, 667.2 (15) $[M - 2PF_6 - 2F]^{2+}$, 648.2 (<5) $[M - 2PF_6 - 4F]^{2+}$.

Anal. Calcd for $C_{80}H_{72}B_2F_{16}N_{10}RuP_2$: C, 57.81; H, 4.37; N, 8.43. Found: C, 57.55; H, 4.53; N, 8.63.

Acknowledgment. This research was supported by the CNRS, le Ministère de la Recherche et des Nouvelles Technologies, the IST/ILO (EC Contract 2001-33057), MIUR (PRIN 2003 on Artificial Photosynthesis) and FIRB (Contract no. RBNE019H9K).

Supporting Information Available: A figure showing the nanosecond transient absorption spectrum and decay of **6** in acetonitrile at room temperature. This material is available free of charge via the Internet at http://pubs.acs.org.

References and Notes

(1) Balzani, V.; Credi, A.; Venturi, M. *Molecular Devices and Machines*; Wiley-VCH: Weinheim, 2003; Chapters 2−6 and references therein.

(2) This topic is too vaste to be exhaustively quoted. For recent review articles, see: (a) Paddon-Row, M. N. In: *Electron Transfer in Chemistry*; Balzani, V., Ed.; Wiley-VCH: Weinheim, 2001; Vol. 3, pp 179−271 (see also references therein). (b) Wasielewski, M. R. *Chem. Rev.* **1992**, *92*, 435. (c) Barbara, P. F.; Meyer, T. J.; Ratner, M. A. *J. Phys. Chem.* **1996**, *100*, 13148−13168.

(3) This topic is too vast to be exhaustively quoted. For recent review articles, see: (a) Gust, D.; Moore, T. A.; Moore A. L. In *Electron Transfer in Chemistry*; Balzani, V., Ed.; Wiley-VCH: Weinheim, 2001; Vol. 3, pp 272−336 (see also references therein). (b) Scandola, F.; Chiorboli, C.; Indelli, M. T.; Rampi, M. A. In *Electron Transfer in Chemistry*; Balzani, V., Ed.; Wiley-VCH: Weinheim, 2001; Vol. 3, pp 337−408 (see also references therein). (c) Hsiao, J.-S.; Krueger, B. P.; Wagner, R. W.; Johnson, T. E.; Delaney, J. K.; Mauzerall, D. C.; Fleming, G. R.; Lindsey, J. S.; Bocian, D. F.; Donohoe, R. J. *J. Am. Chem. Soc.* **1996**, *118*, 11181−11193. (d) Campagna, S.; Serroni, S.; Puntoriero, F.; Di Pietro, C.; Ricevuto, V. In *Electron Transfer in Chemistry*; Balzani, V., Ed.; Wiley-VCH: Weinheim, 2001; Vol. 3, pp 186−214 (see also references therein). (e) De Cola, L.; Belser, P. *Coord. Chem. Rev.* **1998**, *177*, 301. (f) Harriman, A.; Ziessel, R. *Coord. Chem. Rev.* **1998**, *171*, 331. (g) Barigelletti, F.; Flamigni, L. *Chem. Soc. Rev.* **2000**, *29*, 1. (h) Sun, L.; Hammarström, L.; Akermark, B.; Styring, S. *Chem. Soc. Rev.* **2001**, *30*, 36. (i) Harriman, A. *Angew. Chem., Int. Ed.* **2004**, *43*, 4985. (j) Baranoff, E.; Collin, J.-P.; Flamigni, L.; Sauvage, J.-P. *Chem. Soc. Rev.* **2004**, *33*, 147−155. (k) Alstrum-Acevedo, J. H.; Brennaman, M. K.; Meyer, T. J. *Inorg. Chem.* **2005**, *44*, 6802−6827. (l) Browne, W. R.; O'Boyle, N. M.; McGarvey, J. J.; Vos, J. G. *Chem. Soc. Rev.* **2005**, *34*, 641−663. (m) Chakraborty, S.; Wadas, T. J.; Hester, H.; Schmehl, R.; Eisenberg, R. *Inorg. Chem.* **2005**, *44*, 6865−6878.

(4) Balzani, V.; Scandola, F. *Supramolecular Photochemistry*; Horwood: Chichester, U.K., 1991.

(5) (a) Lainé, P.; Bedioui, F.; Amouyal, E.; Albin, V.; Berruyer-Penaud, F. *Chem. Eur. J.* **2002**, *8*, 3162−3176. (b) Lainé, P.; Bedioui, F.; Ochsenbein, P.; Marvaud, V.; Bonin, M.; Amouyal, E. *J. Am. Chem. Soc.* **2002**, *124*, 1364−1377. (c) Ciofini, I.; Lainé, P. P.; Bedioui, F.; Adamo, C. *J. Am. Chem. Soc.* **2004**, *126*, 10763−10777.

(6) Haugland, R. P. *Handbook of Molecular Probes and Research Products*, 9th ed.; Molecular Probes, Inc.: Eugene, OR, 2002.

(7) Burghart, A.; Kim, H.; Wech, M. B.; Thorensen, L. H.; Reibenspies, J.; Burgess, K. *J. Org. Chem.* **1999**, *64*, 7813.

(8) Thoresen, L. H.; Kim, H.; Welch, M. B.; Burghart, A.; Burgess, K. *Synlett* **1998**, 1276.

(9) Chen, T.; Boyer, J. H.; Trudell, M. L. *Heteroatom Chem.* **1997**, *8*, 51.

(10) Sathyamoorthi, G.; Wolford, L. T.; Haag, A. M.; Boyer, J. H. *Heteroatom Chem.* **1994**, *5*, 245.

(11) Gareis, T.; Huber, C.; Wolfbeis, O. S.; Daub, J. *Chem. Commun.* **1997**, 1717.

(12) Kollmannsberger, M.; Rurack, K.; Resch-Genger, U.; Daub, J. *J. Phys. Chem.* **1998**, *102*, 10211.

(13) Rurack, K.; Kollmannsberger, M.; Resch-Genger, U.; Daub, J. *J. Am. Chem. Soc.* **2000**, *122*, 968.

(14) Turfan, B.; Akkaya, E. U. *Org. Lett.* **2002**, *4*, 2857.

(15) Goze, C.; Ulrich, G.; Charbonnière, L.; Ziessel, R. *Chem. Eur. J.* **2003**, *9*, 3748.

(16) Li, F.; Yang, S. I.; Ciringh, Y.; Seth, J.; Martin, C. H., III; Singh, D. L.; Kim, D.; Birge, R. R.; Bocian, D. F.; Holten, D.; Lindsey, J. S. *J. Am. Chem. Soc*. **1998**, *120*, 10001.

(17) Burghart, A.; Thoresen, L. H.; Che, J.; Burgess, K.; Bergström, F.; Johansson, L. B.-Å. *Chem. Commun*. **2000**, 2203.

(18) (a) Crosby, G. A. *Acc. Chem. Res.* **1975**, *8*, 231. (b) Meyer, T. J. *Pure Appl. Chem.* **1986**, *58*, 1193. (c) Juris, A.; Balzani, V.; Barigelletti, F.; Campagna, S.; Belser, P.; Von Zelewsky, A. *Coord. Chem. Rev.* **1988**, *84*, 85.

(19) Serroni, S.; Campagna, S.; Puntoriero, F.; Di Pietro, C.; McClenaghan, N. D.; Loiseau, F. *Chem.* Soc. Rev. **2001**, *30*, 367. Schubert, U. S.; Eschbaumer, C. *Angew. Chem., Int. Ed*. **2002**, *41*, 2893.

(20) Galletta, M.; Campagna, S.; Quesada, M.; Ulrich, G.; Ziessel, R. *Chem. Commun.* **2005**, 4222.

(21) Ulrich, G.; Ziessel, R. *J. Org. Chem.* **2004**, *69*, 2070.

(22) Sullivan, B. P.; Salmon, D. J.; Meyer, T. J. *Inorg. Chem*., **1978**, *17*, 3334.

(23) Ziessel, R.; Grosshenny, V.; Hissler, M.; Stroh, C. *Inorg. Chem*. **2004**, *17*, 4262.

(24) (a) Klessinger M.; Michl, J. *Excited States and Photochemistry of Organic Molecules*; VCH: New York, 1995. (b) *Handbook of Photochemistry*, 3rd ed., Revised and Expanded; Montalti, M., Credi, A., Prodi, L., Gandolfi, M. T., Eds.; CRC Press: Boca Raton, FL, 2006.

(25) Karolin, J.; Johansson, L. B.-A.; Strandberg, L.; Ny, T. *J. Am. Chem. Soc*. **1994**, *116*, 7801.

(26) Alternatively, it could be stated that the phenylethynyl group destabilizes the bodipy-centered HOMO.

(27) Marcaccio, M.; Paolucci, F.; Paradisi, C.; Roffia, S.; Fontanesi, C.; Yellowlees, L. J.; Serroni, S.; Campagna, S.; Denti, G.; Balzani, V. *J. Am. Chem. Soc*. **1999**, *121*, 10081 and references therein.

(28) If the complex was homoleptic, the electron pairing energy would be related to the potential difference between the third and fourth reduction process. However, because the other two reduction processes are intermediate between the first and second reductions of the same ligand in **6**, the 540 mV separation value, that is the difference between the first and second reduction processes, does not have an effective significance and eventually can only be considered as a high limit for the potential separation related to electron pairing. The effective electron pairing energy should be related to a significantly lower potential separation value.

(29) (a) Harriman, A.; Romero, F. M.; Ziessel, R.; Benniston, A. C. *J. Phys. Chem. A* **1999**, *103*, 5399. (b) El-ghayoury, A.; Harriman, A.; Khatyr, A.; Ziessel, R. *J. Phys. Chem. A* **2000**, *104*, 1512−1523.

(30) (a) Sauvage, J.-P.; Collin, J.-P.; Chambron, J.-C.; Guillerez, S.; Coudret, C.; Balzani, V.; Barigelleti, F.; De Cola, L.; Flamigni, L. *Chem. Rev.* **1994**, *94*, 993−1019. (b) Balzani, V.; Juris, A.; Venturi, M.; Campagna, S.; Serroni, S. *Chem. Rev.* **1996**, *96*, 759.

(31) Förster, Th. In *Modern Quantum Chemistry*; Sinanoglu, O., Ed.; Academic Press: New York, 1965.

(32) Dexter, D. L. *J. Chem. Phys.* **1953**, *21*, 836.

(33) However, because of the presence of the heavy metal, spin prohibition could not been strictly followed in **1**−**6** and contribution from this route cannot be totally ruled out.

(34) In eq 1, which assumes Koopman's theorem as valid and neglects the work term, $^*E_{ox(bodipy)}$ is the excited-state oxidation potential of the bodipy subunits, in its turn estimated from the equation $^*E_{ox(bodipy)} = E_{ox(bodipy)} - E_{00}/e$, where $E_{ox(bodipy)}$ is the ground-state oxidation potential of the bodipy subunits and E_{00} is the energy of the singlet bodipy-centered fluorescent level.

(35) Gaines, G. L., III; O'Neil, M. P.; Svec, W. A.; Niemczyk, M. P.; Wasielewski, M. R. *J. Am. Chem. Soc*. **1991**, *113*, 719−721.

(36) Femtosecond transient absorption spectroscopy was complicated by photoinstability of the investigated species under the intense laser pulses used. In fact, the free ligands displaced poor photostability under these conditions, which hampered femtosecond spectroscopy investigation of **L1**−**L6**. The metal complexes **1**−**6** exhibited also some photostability problems in several solvents. However, in acetonitrile they were photostable enough to allow the study. Analogous photostability problems were not faced with the nanosecond apparatus, which used a less intense laser pulse.

(37) The ^{1}MLCT state has several possible deactivation routes: (a) intersystem crossing to the ^{3}MLCT state (which should successively deactivate to the bodipy triplet); (b) intercomponent singlet−singlet energy transfer to the bodipy-centered singlet state; (c) oxidative electron transfer leading to the charge-separated state (see also Figure 7). Process (a) is known to occur in the subpicosecond time scale in Ru(II) complexes,[38] so it could seem to be the obvious choice. However, in our case, a careful comparison between the transient absorption and ground-state absorption spectra suggests that processes (b) and (c) can dominate. In fact, because excitation is at 450 nm, the ^{1}MLCT state is preferentially initially formed compared to the $^1\pi-\pi^*$ state (e.g., from a rough estimation based on extinction coefficients, 75% of ^{1}MLCT is initially formed in **5**). At 1 ps from the laser pulse, therefore, one could expect the bleaching in the 450−490 nm region, the range of MLCT absorption band, would be larger than (or at least comparable with) the bleaching of the bodipy-centered absorption. This would, in fact, be the case if most excitation resides on the ^{1}MLCT or ^{3}MLCT states. Because transient absorption spectra (see Figure 8) only show from moderate to negligible MLCT bleaching compared to the bleaching of the bodipy-centered absorption band, we assume that the main deactivation routes of ^{1}MLCT are (b) and/or (c). Actually, both ultrafast (on a femtosecond time scale) singlet−singlet energy transfer[39] and photoinduced oxidative electron-transfer involving singlet states[40] have been recently observed in particular Ru(II) complexes. We also report that one of the referees made some objections on the ultrafast singlet−singlet energy transfer route (b). We believe that his/her concern is essentially due to the fact that this process has only been rarely reported up to now in multicomponent species involving transition metal complexes. But the experimental results in our hands strongly point toward this interpretation, and we decided to keep it. However, we felt that the readers should know this objection.

(38) (a) Bradley, P. C.; Kress, N.; Hornberger, B. A.; Dallinger, R. F.; Woodruff, W. H. *J. Am. Chem. Soc*. **1989**, *111*, 7441. (b) Yeh, A. T.; Shank, C. V.; McCusker, J. K. *Science* **2000**, *289*, 935.

(39) (a) Andersson, J.; Puntoriero, F.; Serroni, S.; Yartsev, A.; Pascher, T.; Polivka, T.; Campagna, S.; Sundström,V. *Chem. Phys. Lett.* **2004**, *386*, 336−341. (b) Andersson, J.; Puntoriero, F.; Serroni, S.; Yartsev, A.; Pascher, T.; Polivka, T.; Campagna, S.; Sundström, V. *Faraday Discuss.* **2004**, *127*, 295.

(40) (a) Moser, J. E.; Grätzel, M. *Chimica* **1998**, *52*, 160. (b) Kallioinen, J.; Benkö, G.; Sundström, V.; Korppi-Tommola, J. E.I.; Yartsev, A. P. *J. Phys. Chem. B* **2002**, *106*, 4396.

(41) Demas, J. N.; Crosby, G. A. *J. Phys. Chem.* **1971**, *75*, 991.